Polymer 62 (2015) A1–A13

Contents lists available at ScienceDirect

Polymer

journal homepage: www.elsevier.com/locate/polymer

Feature article

Design of block copolymer micelles via crystallization

Jérôme J. Crassous [a], Peter Schurtenberger [a], Matthias Ballauff [b, c], Adriana M. Mihut [a, *]

[a] Division of Physical Chemistry, Department of Chemistry, Lund University, Getingevägen 60, 22100 Lund, Sweden
[b] Soft Matter and Functional Materials, Helmholtz-Zentrum Berlin für Materialien und Energie GmbH, Glienicker Strasse 100, 14109 Berlin, Germany
[c] Department of Physics, Humboldt University Berlin, Newtonstr. 15, 12489 Berlin, Germany

ARTICLE INFO

Article history:
Received 7 November 2014
Received in revised form
28 January 2015
Accepted 17 February 2015
Available online 25 February 2015

Keywords:
Block copolymer crystallization
Block copolymer micelles
Silica nanoparticles
Crystalline-coil
Self-seeding
Crystallization driven self-assembly(CDSA)
Anisotropic structures

ABSTRACT

This Feature Article provides an overview of the progress made over the last few years in the design of diblock copolymer micelles based on *crystallization-driven self-assembly* (CDSA) towards the development of novel and fascinating morphologies with crystalline-cores. Here, we describe the different approaches employed in order to engineer a large variety of semicrystalline micellar architectures. We highlight kinetic strategies that have been employed to direct morphological transitions, which can then be further tuned thus increasing the range of possible micellar structures. We then emphasize the development of complex hybrid assemblies generated by taking advantage of the self-assembly process of crystalline-corona di-BCP micelles with colloidal particles. Each section introduces and emphasizes the potential applications of this class of nanomaterials.

1. Introduction

The ability of diblock copolymers (di-BCPs) to spontaneously organize into a wide range of morphologies, including many complex or hierarchical assemblies, has attracted significant attention due to their potential use in the development of nanomaterials with controlled structures and tunable properties for different applications [1,2]. Remarkably, the successful preparation of micelles from crystalline-coil BCPs by crystallization-driven self-assembly (CDSA) showed over the last ten years that semicrystalline BCPs are very appealing candidates for the development of materials with complex architectures. As a matter of fact, the self-assembly or the micellization of non-crystalline BCPs in solution is well-documented and very good agreement has been established between the experimental and theoretical studies [3–14]. Selective solvation gives rise to the formation of micelles with a core consisting of the insoluble block that is surrounded by a corona formed by the soluble block [10,15]. The resulting structures will depend on the intrinsic molecular parameters of the BCP such as the solubility, the relative volume fraction and the length of the blocks.

The degree of complexity of the self-assembly process is enhanced when one block of the di-BCP is able to crystallize. While the crystallization of BCPs in melt, bulk and thin films has been intensively studied and is well-established [18–31], the crystallization behavior of BCPs in solution still presents many unanswered questions, and the fundamental understanding of the self-assembly mechanism of semicrystalline micelles is far from complete. For the semicrystalline BCPs where the insoluble block is able to crystallize in a selective solvent, the crystal packing forces play a dominant role in determining the morphology of the core objects that are formed [16]. Crystallization-driven self-assembly (CDSA) has emerged as a powerful method for block copolymer architecture manipulation. Recent advances in BCP synthesis, enriched by the development of self-assembly schemes, provided access to a rich collection of semicrystalline BCP micelles. A variety of morphologies consisting of crystalline core-forming micelles has been lately reported for different di or tri-BCP [17,32–67].

In this article, we focus our attention on recent developments in the fabrication and manipulation of semicrystalline diblock copolymer micelles. In Section 2, we discuss self-assembly approaches and mechanisms which result in the formation of micelles with a crystalline-core. Here, the main focus remains on the large variety of architectures available from semicrystalline BCPs and the role played by the crystallization process in the structure development. Also, we illustrate different morphological transitions encountered

* Corresponding author.
E-mail address: adriana.mihut@fkem1.lu.se (A.M. Mihut).

http://dx.doi.org/10.1016/j.polymer.2015.02.030
0032-3861/

by semicrystalline BCP micelles, where the competition between the crystallization of the micellar core and the stretching of the corona block results in unique and interesting micellar structures. Section 3 presents the directed self-assembly of colloidal particles through an underlying controlled crystallization process of micelles with a crystalline corona that leads to the development of hybrid inorganic-organic materials. Finally, some perspectives in the field of semicrystalline BCP micelles are briefly discussed.

2. Design of crystalline core-micelles: general pathways of crystallization-driven self-assembly (CDSA)

2.1. General aspects of semicrystalline di-BCP micelle formation: guiding assembly in selective solvents

In the current section we present a brief outline of the factors that govern semicrystalline di-BCP micelle formation, and we summarize various self-assembly strategies applied to develop a large number of unique and interesting morphologies as illustrated in Fig. 1.

In solution, the interactions between the solvent and the different blocks dictate the ability to form well-defined micellar structures. Often, the formation of semicrystalline BCP micelles can be viewed as a two-step self-assembly process. Micelles with an amorphous insoluble core-forming block develop by minimizing their contact with the solvent, and then start to crystallize in a second step, giving rise to the final micellar structure. As a general rule, the geometry and degree of order of these architectures depend not only on the molecular characteristics of the BCP, but also on the ratio between the insoluble and the soluble blocks. As crystallization takes place in the insoluble micellar core, the initial morphology is either preserved or a morphological transformation/development into a novel structure is triggered through a reorganization process as shown in Fig. 1. Therefore, the structure development of BCPs in solution will depend on two competing self-organizing mechanisms: microphase separation and crystallization.

From the theoretical point of view, Vilgis and Halperin established a scaling analysis for the morphology development of semicrystalline di-BCPs in selective solvents in which the insoluble block can crystallize [16]. According to this model, the insoluble and crystallizable block forms crystals through adjacent folds within the core, and a sharp interface divides the crystalline core from the solvent-swollen corona. The corona chains are grafted to the core at a spacing that depends on the number of folds per core block. Thus, the response to strong corona chain repulsion is a large number of thinner folds of the crystallizable core-forming block. The core crystallinity affects the equilibrium state of the resulting structure as follows: in a first step crystallization determines the packing mode of the core block (by inducing chain folding), and sets the relationship between the grafting density of the amorphous block and the core geometry. As a direct consequence, the crystallization gives rise to two different surface tensions associated with the chain fold. The first one arises from the interfacial tension in the fold plane, while the second characterizes the lateral interfacial tension at the edge of each crystal. From this model, the most common morphology expected is a lamellar structure where the corona chains protrude from both faces. In the case of a very long soluble block, cylindrical or even star-like micelles are expected (see Fig. 1a). Because the core is formed by adjacent folds of the crystalline polymer, the core of the semicrystalline micelles does not have a circular cross section but is rather formed by an end-to-end packing of a rectangular unit cell.

Experimentally, different approaches have been employed for coil-crystalline di-BCPs in order to obtain semicrystalline micelles as schematically summarized in Fig. 1. Here, crystallization is the main driving force for solution self-assembly of the di-BCPs. In this way, a large variety of morphologies were prepared by adjusting parameters such as the crystallization conditions, the micelle concentration or the volume ratio between insoluble and soluble

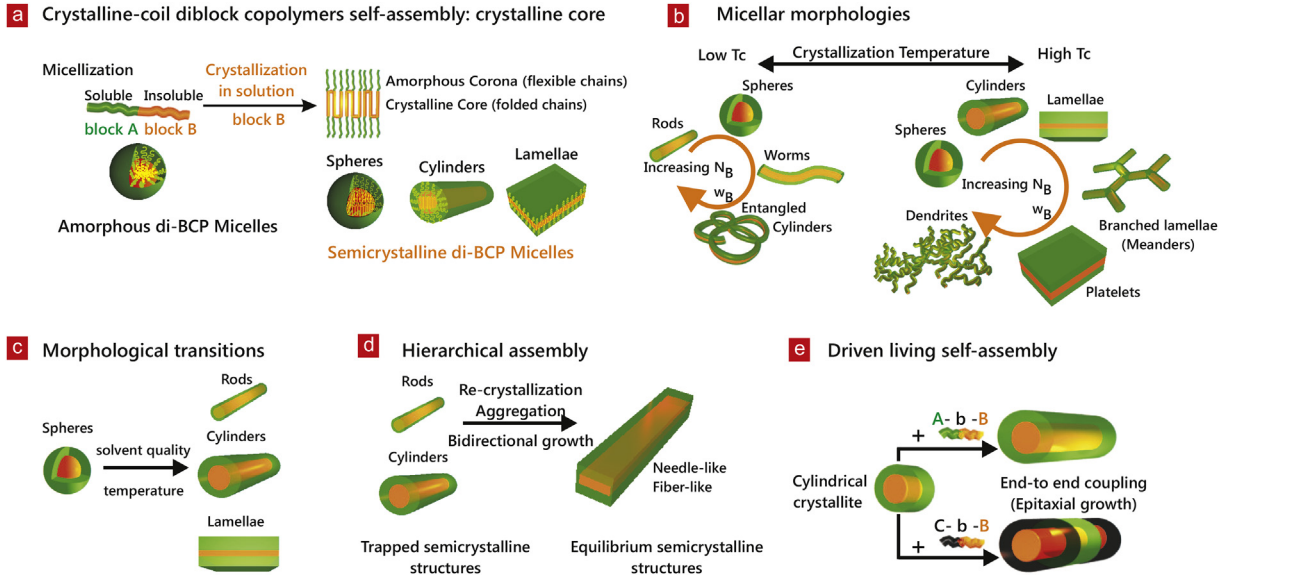

Fig. 1. Different self-assembly strategies to prepare semicrystalline micelles with a crystalline core: a) Schematic illustration of the fabrication of semicrystalline BCP micelles from amorphous micelles in solution where the chains of the core-forming block undergo crystallization through a folded-chain structure as predicted by Vilgis and Halperin [16]. The A and B diblock copolymer, is depicted as a simple two-color chain for simplicity. Typical structures of semicrystalline BCPs micelles: spheres, cylinders and lamellae. b) Representative morphologies formed from PB-*b*-PEO in *n*-heptane as a function of molecular size and composition. The concept of this figure originates from Ref. [17] c) By altering the solubility of the corona-forming blocks in the solvent, the resulting micellar morphology can be further tuned. d) Structures formed from kinetically trapped semicrystalline micelles resulting from the re-crystallization and aggregation of the intermediate structures. e) Micellar morphologies obtained by epitaxial crystallization process, where the addition of extra crystallizable BCP-unimers to the highly reactive crystal surfaces that are present in solution leads to a living type extension of the micellar structure. This concept is discussed in details in Section 2.5.

blocks, the extra addition of crystalline BCP reservoirs, and the solvent selectivity/polarity. Spheres, cylinders and lamellae are the most common morphologies observed. However, by manipulating the interactions between the two blocks and the solvent, and the interplay between the crystallization of the core-forming block and the corona chain stretching, the micellar morphology is no longer restricted to common geometries and complex and hierarchical structures that incorporate desired properties become accessible.

A number of key processes in the context of semicrystalline micelle formation of crystalline-coil di-BCPs have been described in the literature:

- (i) *Thermally controlled crystallization* (Fig. 1b). If the crystallization process can be handled in a controlled way by regulating the crystallization temperature T_c or the choice of the quench depth and rate, a variety of equilibrium structures can be prepared. Here, the crystallization of the micellar core takes place within a confinement, *i.e.*, in a "*frozen*" micelle when the initial melt BCP structure is retained (generally imposed by fast crystallization process at a very low crystallization temperature T_c and a large quench depth/fast quench rate). Otherwise, crystallization allows the development of new distinct features by enabling the breakout from the initial melt BCP structure (through a slow crystallization process occurring at a high crystallization temperature T_c and a small quench depth/slow quench rate). As switching between different architectures is possible when the micellar solutions are heated above the melting temperature T_m of the crystalline block, the micellar morphology is no longer restricted to the microphase separation of the BCPs [17,32–34,52,56,58,68].
- (ii) *Morphological transitions* (Fig. 1c). The micellar morphology also depends on the solvent quality, where the competition between the stretching of the chain of the soluble block and the crystallization energy of the core-forming block sets the micellar shape boundaries. Even if crystallization occurs in the micellar core and plays the major role in determining the micellar structure, an additional deterioration of the solvent quality for the chain of the corona micelles, *i.e.*, a change in conformation of the soluble block, will favor further morphological transitions. Not only the solvent quality can alter the micellar structure, but transitions can be also brought out solely by a change of the temperature [35,44,45,57,69–73].
- (iii) *Hierarchical assembly* (Fig. 1d). Equilibrium structures may be generated from the re-organization and re-crystallization of kinetically trapped metastable crystalline micellar structures. These metastable crystalline micelles generated at an earlier stage of the core crystallization can experience an aggregation process either by fusion or coalescence, that is accompanied by a secondary crystallization which ultimately favors the development of much larger and stable structures. In addition to the improved solvation conditions of the core-forming block, the low crystallinity of the initial crystalline micelles is believed to be the main responsible for rearrangements and recrystallization events [44,45,57,70–74].
- (iv) "*Living*" *crystallization* (Fig. 1e). This approach relies also on a self-assembly process where the micelle formation is driven by the crystallization of the core forming block. Distinct from the previous methods is the living character of the CDSA process as the growth of the semicrystalline micelles can be generated by elongation via an epitaxial growth process. Here, the ends or edges of pre-crystallized seed micelles remain active to the addition of further polymer unimers, and controlled elongation is possible. This process proved to be a very efficient way for the preparation of well-defined structures with an additional control over the micellar length and morphology [49,50,66,74–79].

The most common crystallized blocks in these micelles are composed of poly(ethylene oxide) (PEO) [17,56–58], poly(ε-caprolactone) (PCL) [32,33,35,68,69,79], polyethylene (PE) [34,52] and poly(ferro-cenyldimethylsilane) (PFS) [49,50,74–78]. Each of these approaches are discussed later in more details.

2.2. Thermally controlled crystallization-induced self-assembly

In what follows we refer to one of the straightforward methods to achieve micellar crystalline morphologies, *i.e.*, the manipulation of the crystallization condition for the semicrystalline core-forming block (see Fig. 2). Here, the structure formation of micelles generally starts by dissolving the di-BCP in a selective solvent at temperatures above the melting temperature T_m of the crystallizable block. In this first step the geometry of the amorphous micelles depends on the concentration and the volume/length ratio between insoluble and soluble blocks, imposed by the packing parameter as the ratio between the insoluble chain molecular volume and the volume occupied by the copolymer assembly. In a second step, when the polymer solutions are cooled down to different crystallization temperatures T_c, below the melting temperature T_m, crystallization occurs. The lowering of temperature below T_m is accompanied by a further degradation of the solvent quality for the crystallizable block. The key parameter in order to tune the morphology by this method are the appropriate choice of the crystallization conditions. Here, the crystallization temperature T_c and/or the temperature quenching depth/rate can be varied for the core-forming block by initiating the crystallization process by:

- fast quenching: shallow (high T_c) or deep (very low T_c) quench with very high cooling rate
- slow quenching: shallow quench (high T_c) with low cooling rate

This method allows for a unique chance to control the micellar crystal development with respect to starting crystallization time, nucleation rate and growth direction.

Mihut and co-workers have recently reported a morphological phase map of semicrystalline poly(butadiene)-*block*-poly-(ethylene oxide) (PB-*b*-PEO) di-BCPs micelles in dilute *n*-heptane solutions [17]. The interplay between the crystallization of the PEO block and the self-assembly behavior, as a function of the molecular composition of the di-BCP, is the key feature that allows the access to a large variety of semicrystalline micelles as displayed by the schematic drawings in Fig. 1b and by the selected examples in Fig. 2a–e. Here, micelles consisting of a crystalline PEO core and a soluble PB corona were generated though the thermally controlled crystallization of the PEO block, *via* two crystallization pathways, that is: by fast quenching to the temperature of liquid nitrogen and by slow quenching to the crystallization temperature of the PEO block.

When crystallization takes place at low temperatures, the spherical morphology present in the molten state was mostly preserved in the BCPs with a weight fraction composition of the PEO block, w_{PEO}, below or equal to 0.58, whereas above 0.58 worm-like and entangled cylindrical micelles were obtained. On the other hand, morphological transitions from spheres to lamellar structures were observed upon crystallization at the T_m of PEO block, above $w_{PEO} = 0.32$. Hereby, the morphology present in the molten state is perturbed due to a breakout crystallization. Additionally, both thermal pathways exhibit coexistence regions of mixed populations of either rods + spheres, worms + spheres, cylinders + platelets and lamellae + platelets in the broad range of 0.38–0.58 (see Fig. 2e). X-ray diffraction (XRD) analysis indicated that the degree of crystallinity of these micelles strongly depends on the crystallization kinetics and the crystal growth mechanism enabled through either a confined or a breakout crystallization.

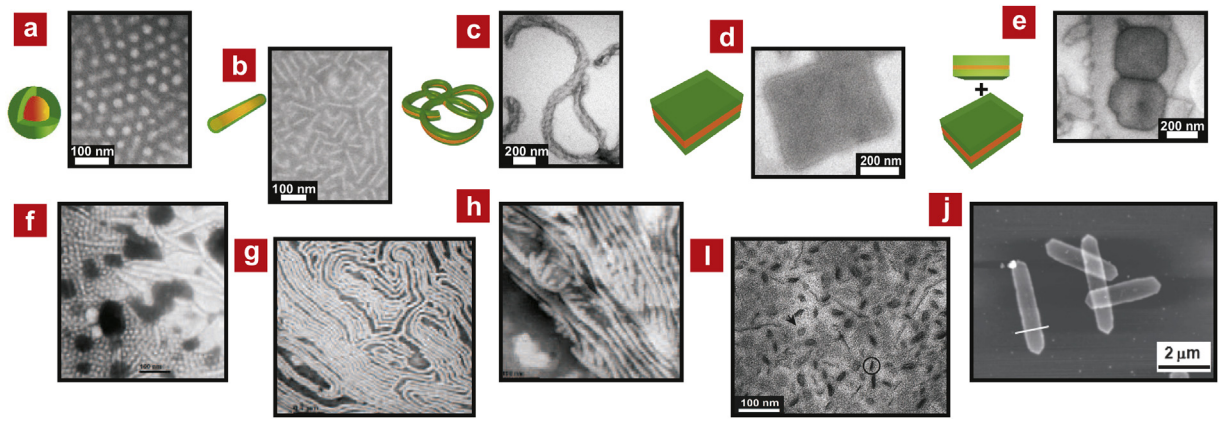

Fig. 2. Selected examples of semicrystalline micelles with a crystalline core: (a) spheres, (b) rods, (c) entangled cylinders, (d) platelets, (e) platelets and lamellae from poly(-butadiene)-*block*-poly(ethylene oxide) (PB-*b*-PEO) BCP in *n*-heptane solutions containing a crystalline PEO core (Adapted from Ref. [17] with permission; Copyright 2012 The Royal Society of Chemistry); (f) spheres and cylinders (g) wormlike (h) bandlike lamellae from poly(ε-caprolactone)-*block*-poly(ethylene oxide) (PCL-*b*-PEO) BCP in aqueous solutions containing a PCL crystalline core (Reprinted with permission from Ref. [32] and Ref. [33]; Copyright 2008 WILEY-VCH Verlag GmbH & Co. KGaA, Weinheim, and 2007 American Chemical Society, respectively.); (i) disklike from poly(*N*,*N*-dimethylacrylamide)-polyethylene (PDMA-PE) BCP in aqueous solutions containing a PE crystalline core (Reprinted with permission from Ref. [52]; Copyright 2011 American Chemical Society) (j) lamellae with elongated truncated lozenge-like shape single crystals from poly(2-vinylpyridine)-*block*-poly(ε-caprolactone) (P2VP-*b*-PCL) in DMF/water mixture containing a PCL crystalline core (Reprinted with permission from Ref. [68]; Copyright 2013 WILEY-VCH Verlag GmbH & Co. KGaA, Weinheim).

The length of the crystallizable PEO block has also an influence on the micellar morphology as theoretical predicted by Vilgis and Halperin [16]. An increase of the PEO block content favors morphological transitions from spheres to cylinders, lamellae and platelet-like structures. The increase of the PEO length and w_{PEO} promotes an increase of the packing parameter, *i.e.*, the number of folded PEO chains in the crystalline core. Thus, smaller lamellar thickness are favored at large fold numbers in the PEO crystals due to the strong repulsion and the sharp interface between the PEO core and the solvent-swollen PB corona. In this case, the lamellae thickness is governed by a balance between the entropic contribution due to the stretching of the solvated chains and the enthalpic contribution due to folding of the crystalline chains in the lamellae.

This self-assembly method has the advantage of being fully reversible, *i.e.*, once the di-BCPs solutions are heated above the melting temperature T_m of the crystalline PEO block, the system recovers its original amorphous state. Such di-BCPs are highly versatile systems, as two distinct micellar morphologies can be obtained by simply switching between two thermal crystallization pathways without the requirement of a solvent exchange, and any additional chemistry or polymer synthesis.

Using a similar approach, investigations by Du and co-workers on a poly(ε-caprolactone)-*block*-poly(ethylene oxide) (PCL-*b*-PEO) BCP in water showed that the morphology can be influenced by the crystallization temperature, due to an increased chain folding at lower crystallization temperature T_c [32]. Lamellar micelles are formed at a higher crystallization temperature for PCL-*b*-PEO BCP which have a shorter soluble PCL block, while spherical micelles or cylindrical micelles tend to be formed at a lower T_c. The lamellar micelles consist of PCL crystals sandwiched between PEO brushes. In this case, the morphology is mainly dictated by the perfection of the crystals in the micellar core. For the BCP containing a longer soluble block, the micellar morphology is determined by the tethering density of the soluble PEO chains. Spherical micelles or cylindrical micelles with a larger length/diameter ratio were formed at higher T_c, due to a decrease of the chain folding number and an increase of the grafting density of the soluble PEO chains on the PCL crystal surface. Otherwise, lower T_c for the same BCP led to the formation of lamellar or cylindrical micelles with a smaller length/diameter. Special attention has been paid by the same authors, to the development of micellar morphology and size of the PCL-*b*-PEO micelles as a function of the lengths of the blocks and composition [33]. It was observed that as the length of the crystalline PCL core-forming block increases, the micellar morphology changes from spherical, rod-like, worm-like to lamellar structures. As mentioned previously, the micellar morphology can be correlated with the reduced tethering density which has been determined by the number of the chain folds of the PCL core and the random coil size of the soluble PEO corona. Large tethering densities and a longer chain length of the soluble PEO corona favor the formation of spherical micelles. At the same time, an increase of the PCL block length means an increase of the chain folding number and a decrease of the tethering density. Thus, morphological transitions from spherical to lamellar micelles were preferred in solution (see Fig. 2f–h).

Yin et al. successfully prepared a sequence of BCP micelles from poly(*N*,*N*-dimethylacrylamide)-polyethylene (PDMA-PE) in water [34,52]. Oblate ellipsoids, wormlike micelles and bilayer vesicles were generated by changing the composition of the PDMA-PE BCP. Prior to crystallization, the micellar aggregates consist of a PE molten core. No morphological transition was observed on the overall structure of the aggregates after the PE core crystallized at 25 °C. A combination of cryogenic transmission electron microscopy (cryo-TEM) and small angle neutron scattering (SANS) analysis indicated the development of micellar cores in which crystalline PE exists as disks at the center, sandwiched by amorphous PE on both sides. The overall structure of the core was approximated as an oblate ellipsoid. Yin and Hillmyer also reported a morphological transition driven by the crystallization of the PE-core forming block of the poly(*N*,*N*-dimethylacrylamide)-polyethylene (PDMA-PE) di-BCP in water [52]. By cooling down the polymer solution from 120 °C, that is above the T_m of the PE block, to 25 °C, disklike micelles formed *via* a confined PE crystallization that took place in each frozen micelle, in contrast to the spherical micelles observed from a control sample with amorphous rubbery poly(ethylene-*alt*-propylene) (PEP) as the core-forming material (see Fig. 2i).

Recently, Su and co-workers revealed that thermally controlled crystallization is a facile approach for the direct formation of single crystals of poly(2-vinylpyridine)-*block*-poly(ε-caprolactone) (P2VP-*b*-PCL) BCP in micellar system as shown in Fig. 2j and can be seen as

an elegant alternative to the self-seeding method (see the detailed discussion on the self-seeding method in Section 2.5) [68]. Truncated lozenge-shaped single crystals consisting of a PCL single crystal sandwiched between two P2VP amorphous layers, were prepared at 20 °C by adding water into a dilute DMF solution of the copolymer. The authors observed that the structure formation strongly depends on the crystallization temperature and the solvent quality. They found that when crystallization occurs at a lower temperature (10 °C), the preferential direction of crystal growth becomes weaker and the crystal growth can proceed in all planes, resulting in a slight increase both in length and width of the crystals. On the contrary at temperatures higher than 20 °C, the crystallization process is hindered, and only spherical amorphous micelles were attained in solution at 30 °C.

2.3. Mechanism of crystallization

Understanding how the core-forming block crystallizes is a key requirement for tailoring the resulting morphologies into desired geometries. Important insights of the crystalline nature and the crystals growth mechanism have been provided over the time by scattering techniques such as small- (SAXS) and wide-angle X-ray scattering (WAXS), dynamic (DLS) and static light scattering (SLS).

The formation mechanism of micellar structures *via* a CDSA process was systematically investigated in the work of Mihut et al. by time-resolved WAXS and time-resolved cryo-TEM [56]. The growth mechanism of a 2D meander-like structure of PB-*b*-PEO BCP in *n*-heptane was found to occur *via* a crystallization-induced aggregation process of spherical micelles which were present in the melt upon cooling at the crystallization temperature, $T_c = 30$ °C, of the PEO-core forming block (Fig. 3, Fig. 4). The micelles started to aggregate and immediately became crystalline upon merging with the primary crystalline nucleus. In this case, the primary nucleation point starts in the micellar structure and is followed by the propagation of the crystallization front at well-defined angles between two subsequent micelles. This rapid aggregation process leads to a depletion of the micelles around the growing crystalline core, leading to a branched 2D lamellar structure referred to as meander-like. In this morphology, the PEO crystalline core resembles a ribbon-like or rectangular prismatic structure having ellipsoidal endings. Moreover, this structure exhibits lateral growth and forms simultaneously two or four branches of equivalent width (Fig. 3). Crystallization-induced aggregation of micellar units has been observed for PB-*b*-PEO BCPs and favored the development of structures as branched lamellae (meanders), platelets and lamellae with platelets (Fig. 3 and Fig. 4c) [17].

Further information about the growth mechanism can be obtained from an Avrami analysis (Fig. 4b). In general, the Avrami exponent *n* is related to the type of nucleation and growth geometry, where $n = 1$ is ascribed to a rod, 2 to a disk-like or lamellae and 3 or 4 to a 3D structure. In this case, *n* is reflecting the rate at which PEO microdomains nucleate. A value of $n = 2.5$ was found for the early stage of the crystallization within the meanders, which implied that the crystals were no longer confined into the microdomaines in which they nucleated, *i.e.*, breakout crystallization occurred upon crystallization which led to the development of a 2D structure. The Avrami exponent of 2.5 indicates that during this thermal pathway, crystallization and aggregation of spherical micelles occurs side-by-side, rather then step-wise as reported for PEO-*b*-PBO blends [80]. In contrast, at a low crystallization temperature $T_c = -30$ °C or large quenching/supercooling of the warm polymer solutions to liquid nitrogen temperature, an Avrami exponent of $n = 0.7$ was found. This crystallization pathway preserved the spherical morphology present in the molten state. Here we are dealing with a confined crystallization process where homogeneous nucleation exclusively took place upon quenching within each individual spherical microdomains,*i.e.*, kinetics are determined by nucleation. The Avrami exponent in this case, reflects the nucleation rate of the PEO in the micellar core. However, it

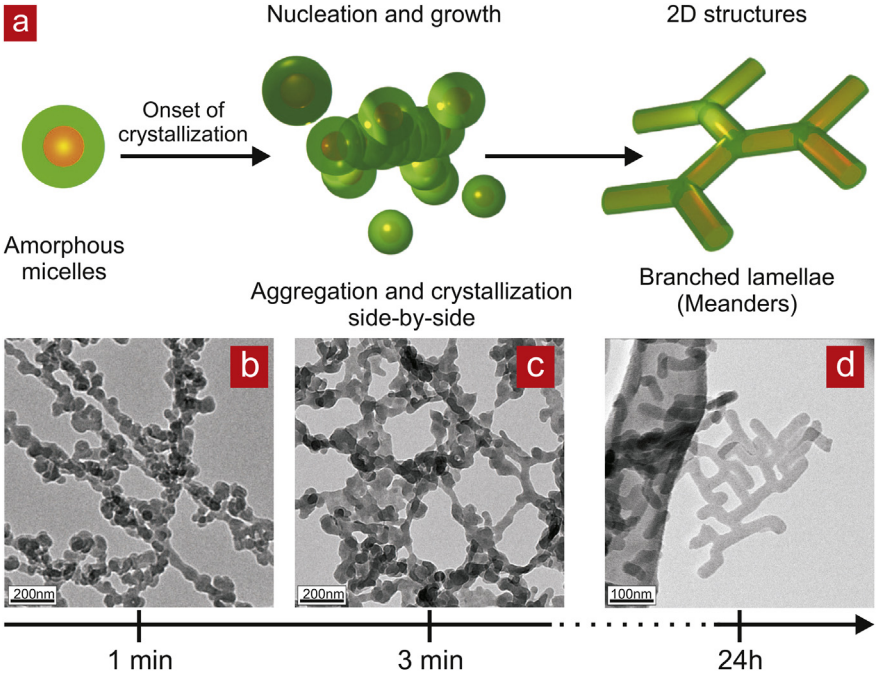

Fig. 3. a) Schematic of the meander-like structure formation by PB_{52}-*b*-$PEO_{48}^{5.6}$ BCP in *n*-heptane *via* a crystallization-induced aggregation of spherical micelles process (the subscripts denote the mass fraction in percent and the superscript gives the overall number average molecular weight of the block copolymer in kg/mol). Cryo-TEM micrographs display the formation of the meander-like structure over time upon cooling the amorphous spherical micelle solution at 30 °C after: 1 min (b), 3 min (c) and 24 h (d). Adapted from Ref. [56]; Copyright 2009 The Royal Society of Chemistry.

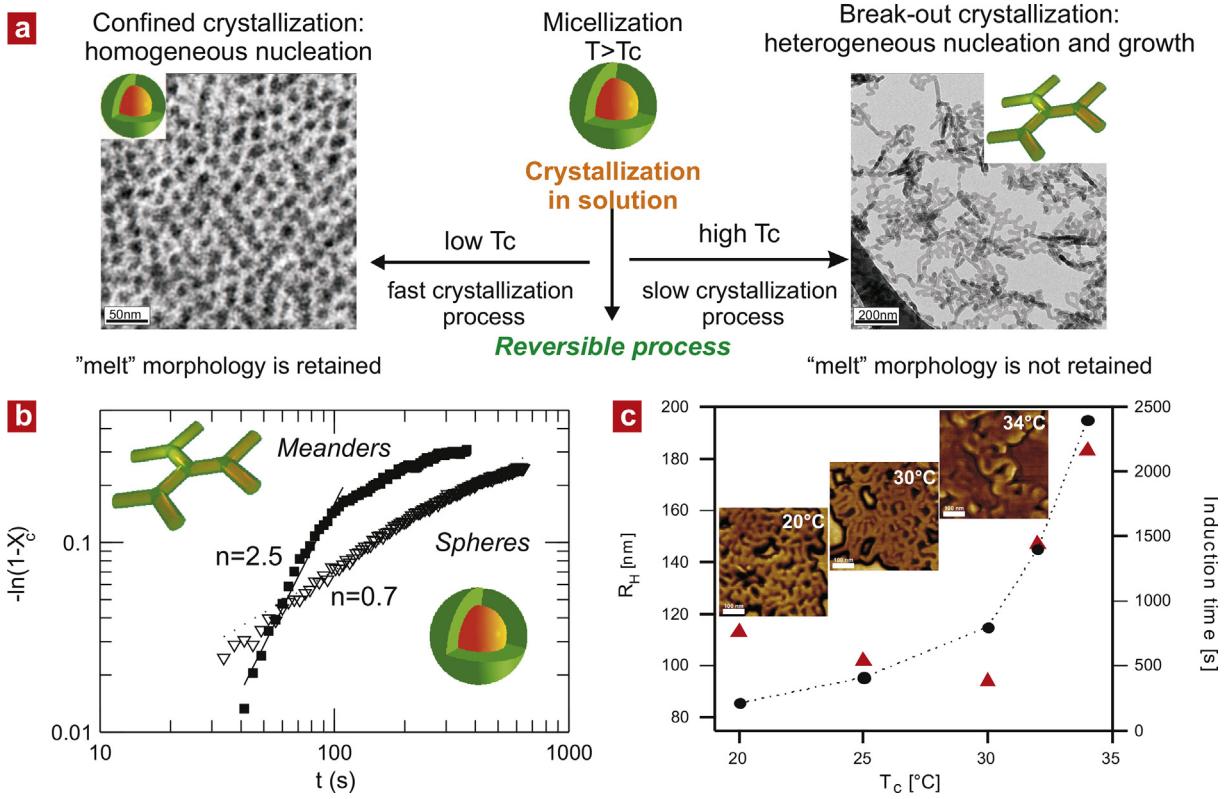

Fig. 4. a) Effect of crystallization, as the main driving force behind the self-assembly of spherical PB-*b*-PEO BCP amorphous micelles, where the prepared samples had two distinct thermal histories. By controlling the crystallization conditions (crystallization temperature T_c, quench depth and rate) the resulting structures can be tuned in a reversible way from spheres to meanders. b) Avrami plots derived from WAXS data for PB_{52}-*b*-$PEO_{48}^{5.6}$ BCP (weight fraction of the PEO block, $w_{PEO} = 0.48$) isothermally crystallized at different T_c: (triangles) spherical micelles, $T_c = -30\,°C$, (squares) meander-like structures, $T_c = 30\,°C$. The dotted line and the full line represent the first degree fits from which the Avrami exponents *n* are obtained. c): Dependence of the size of crystalline micelles (circles with dash line) and of the induction time of the primary nucleation process (triangles) on the crystallization temperature (T_c). The SFM phase images from the inset display the corresponding crystalline morphologies formed by 1 wt% PB_{52}-*b*-$PEO_{48}^{5.6}$ BCP at different T_c: meander-like (20 °C, 30 °C) and twisted lamellae (34 °C). Adapted from Ref. [58]; Copyright 2010 Springer-Verlag.

is worth noting that a low value of the Avrami index is not the only requisite of a homogeneous nucleation process [21]. Related studies have also reported values of the Avrami exponent of 1 or lower when polymers can crystallize under perfect confinement [18,25,30]. A confined crystallization process has been recently found by Yin and Hillmyer for micelles with a crystalline PE-core forming block [52]. Their SANS data confirmed that intermicelle chain exchange of poly(N,N-dimethyl–acrylamide)-polyethylene (PDMA-PE) di-BCP is absent in water at elevated temperature, and thus the crystallization upon cooling took place within each frozen micelle. If to date, homogeneous nucleation has been well-documented for polymers like poly(ε-caprolactone) (PCL) or polyethylene oxide (PEO), for polyethylene (PE) this phenomenon is still under debate. It is in fact believed that it has never been achieved so far since PE crystallizes at much shallower undercooling by surface nucleation [29]. Detailed conditions that are required to encounter homogeneous/heterogeneous or surface nucleation during the crystallization of different polymers have been extensively discussed elsewhere [29–31].

Time- and temperature-dependent light scattering experiments revealed that when crystallization is induced by cooling in the case of PEO as a core-forming block, the crystal morphology depends on the crystallization temperature, T_c. The crystallization process is controlled by two competitive effects, namely, by the nucleation and growth of the PEO core [58]. The kinetics of the crystallization/aggregation process and the size evolution of the aggregates can be monitored by measuring the time dependence of the apparent hydrodynamic radius R_H and of the normalized scattering intensity, I/I_0 after quenching the solutions from above T_m of the PEO block to different T_c. At lower $T_c \leq 30\,°C$, the nucleation rate is high and the crystal growth front is accelerated, which results in a meander-like morphology. In contrast, at higher $T_c \geq 30\,°C$, the nucleation rate was lowered. Due to the reduced number of nuclei/rate, the growth process was slow and no depletion of micelles occurred at the crystal growth front. In this case, the crystal pattern was governed by the growth process rather than the nucleation process. It is reflected in Fig. 4c by the size dependence of the crystalline micelles and the induction time of the primary nucleation process as a function of T_c. Note that the crystal morphology changes from meander-like structures to twisted lamellae within only 4 °C, making this system extremely versatile in terms of accessible structures (see the inset SFM images in Fig. 4c). This change of morphology does not result from a change in the extent of chain folding, as the thickness of the crystals is comparable to that formed at lower T_c.

From this section, we can conclude that crystallization occurs in BCP micelles either in confinement (within the micro-domains already present in the melt) or without confinement (driving structure formation, distinct from the melt structure). It is important to point out that the nucleation and growth events, generally imposed by the choice of the crystallization temperature T_c, are primary factors that set the topological constrains for morphology development. Thus, the competition between the core-forming block crystallization and the self-assembly behavior is the driving force that dictates the morphological development for BCPs containing a crystalline-coil.

2.4. Morphological transitions and hierarchical assembly of semicrystalline micelles

Fine adjustments to the micellization and growth conditions such as solvent quality, crystallization temperature, concentration or sample composition can further alter the initial morphology. In this section, we discuss selected examples exploited by several groups to trigger morphological transitions of semicrystalline di-BCPs micelles. Sphere-to-rod or sphere-to-lamellae transformations of the poly(ε-caprolactone)-*block*-poly(ethylene oxide) (PCL-*b*-PEO) BCP micelles were induced by addition of an inorganic salt, depending on the length of the crystalline PCL block in the BCP as reported by He and co-workers (Fig. 5a,b) [69]. In this system, the formed micelles are composed of a crystalline PCL core and a soluble PEO corona. The spherical micelles are already crystalline before the salt addition. The effect of the inorganic salt on the micellar morphology was interpreted in terms of the "salting-out" effect. Hence, a decrease in the solubility of the PEO chains reduces the tethering density of the corona in the micelles giving rise to micellar transitions in solution. The reduced tethering density is determined by the size of the soluble PEO block and the chain folds of the crystalline PCL block [81]. Therefore, in the presence of salt, the lateral surfaces of the PCL crystals are less covered by the tethered PEO chains. The PCL crystals can then grow into larger crystals, or different spherical micelles aggregate to form lamellar micelles. In the absence of salt, the PEO chains will be overcrowded on the PCL crystals and repel to cover the lateral surface of the crystals. The lateral growth or development into larger morphologies is obstructed and thus spherical micelles are formed. Moreover, He et al. showed that a change of the pH value can drive as well morphological transitions of the semicrystalline PCL-*b*-PEO BCP micelles [35]. The oxygen atoms in the soluble PEO coronar chains can form hydrogen bonds with the H_2O molecules, and therefore the conformation of the PEO block can be altered with pH in the aqueous solution. In alkali solution, the hydrogen bonds are partially destroyed, leading to a reduction of the PEO chain solubility and a collapse of the micellar corona. Thus, the tethering density becomes smaller and leaves some PCL exposed in the spherical micelles as the lateral surface is not fully covered. Therefore, when two neighboring micelles merged, a morphological transition from spheres-to-cylinders occurs in solution. The ability to tailor and control morphological transitions of PCL-*b*-PEO BCPs at low salt concentrations makes these biocompatible and biodegradable BCPs great candidates as drug carriers for controlled release.

A micellar sphere-to-cylinder transition of poly(ferrocenyl dimethylsilane)-*b*-poly(2-vinylpyridine) PFS-*b*-P2VP that led to rather stiff but uniform fiber-like micelles in a selective solvent has been reported by Shen et al. [70]. This structural transformation that occurs at the timescale of weeks is driven by the crystallization of the PFS component in solution. The morphological transformation starts at the early stage with the onset of partial aggregation of spherical micelles. Aggregates coexist with small spherical micelles before the growth of cylindrical or fiber-like micelles. The solvent plays an important role in the nucleation and growth processes of these elongated structures. Not only the solvent quality seems to be an important factor that can induce remarkable morphology transitions in BCP containing a PFS component, but also the ratio between the soluble/insoluble block and the temperature. Transitions from cylindrical (worm-like) micelle to hollow nanotubes were reported [44,45,71,72].

A sphere-to-rod transition of poly(lactide)-b-poly(acrylic acid) (PLA-b-PAA) block copolymers with a short homochiral PLA core forming block has also been reported [82]. The initial spherical micelles slowly crystallized and transformed into crystalline seeds that can further nucleate cylinders growth. Such a process starting from a non-homogeneous solution promotes the development of cylindrical micelles with a large polydispersity in length.

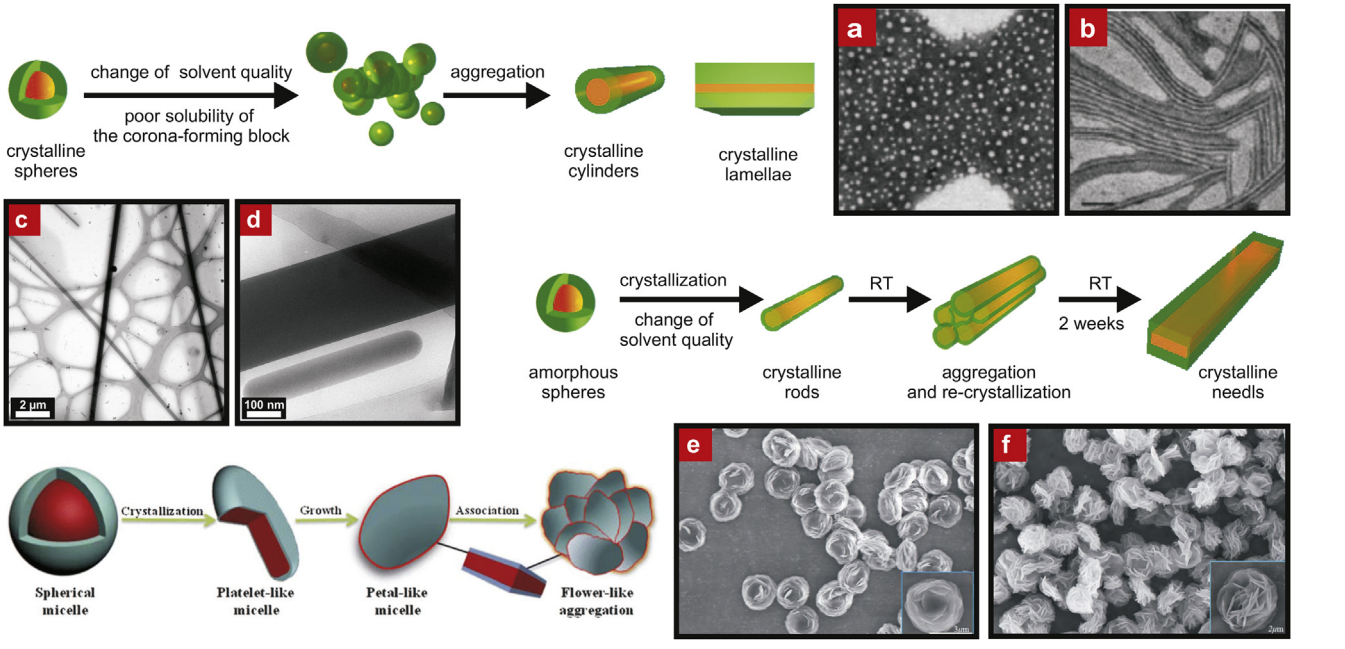

Fig. 5. Proposed mechanism for the morphological transition of semicrystalline PCL-*b*-PEO micelles induced by inorganic salt. Spherical crystalline PCL-*b*-PEO micelles formed in aqueous solution (a) and cylindrical-like micelles formed by addition of NaCl to the aqueous solution containing preformed spherical micelles (b). Reproduced, with permission, from Ref. [69]; Copyright 2010 WILEY-VCH Verlag GmbH & Co. KGaA. Assembly of the semicrystalline PB-*b*-PEO rod-like micelles to needle-like morphology in *n*-heptane (c and d). Reproduced, with permission, from Ref. [57]; Copyright 2010 WILEY-VCH Verlag GmbH & Co. KGaA. Schematic drawing illustrating the self-association mechanism of the *i*PS-*b*-PEG micelles. Reproduced, with permission, from Ref. [73]; Copyright 2013 The Royal Society of Chemistry. Flower-like aggregates of *i*PS-*b*-PEG in DMF after 14 days (e) and after 9 days (f).

Morphological transitions were observed by Mihut et al. through a thermally controlled crystallization of a highly asymmetric PB-*b*-PEO BCP in the selective solvent *n*-heptane, where the amorphous PB block is the major component (Fig. 5c,d) [57]. In this solvent, micellization into a liquid PEO-core and a corona of PB-chains takes place at room temperature. When crystallization occurs at −196 °C (quenching into liquid nitrogen), it leads to a transition from spherical to rod-like micelles. This transition can be explained by a decrease of the solvent quality for the PB-corona chains. Therefore, the PB chains of the micellar corona shrink, occupying less space at the surface of the PEO-core. As a consequence, the spherical micelles become unstable and objects with smaller overall curvature, namely cylinders, are formed. As crystallization starts in the PEO core, the rod-like morphology is preserved when the solution is heated back to room temperature. However, after several weeks, structural changes arise in solution and needle-like structures grow at the expense of the rod-like micelles by fusion or coalescence. The rapid morphological transition from spherical to rod-like micelles leaves some PEO exposed in the rods, favoring a stronger tendency for the rods to thicken and recrystallize leading to more stable structures such as needles. Thus, the low PEO crystallinity of the rods is responsible for the rearrangements and recrystallization at room temperature.

The concept of crystallization-driven self-assembly (CDSA) has been recently extended to weakly polar crystalline BCPs. Li et al. investigated the crystallization behavior of isotactic polystyrene-*b*-poly(ethylene glycol) (*i*PS-*b*-PEG) diblock copolymers in *N*,*N*-dimethylformamide (DMF) solution [73]. Crystallization of the *i*PS core-forming block leads to the formation of micelles upon cooling to room temperature. The authors implied that the formation of the spherical micelles with a gel core cross-linked by the microcrystals of the *i*PS block is related to a slow crystallization process accompanied by a low degree of crystallinity of the micellar core. As crystallinity increases in the micellar core, morphological changes from spherical to plate-like and to petal-like structures are observed over time (Fig. 5e,f). The energy penalty caused by the reduced tethering density of the PEG coronar chains to the *i*PS core surface will further lead to an organization of the unstable petal-like morphology into flower-like aggregates.

2.5. "Living" crystallization-driven self-assembly

Another self-assembly approach is the so-called *living* crystallization-driven self-assembly which has been extensively applied to BCPs with a crystalline core-forming polyferrocenylsilane (PFS) block (Fig. 6). These BCPs are of particular interest due to their potential for a large range of applications such as nanostructured surfaces for magnetic data storage or in surface enhanced Raman scattering (SERS) applications [83–89]. These authors showed during the last past years the great potential and advantage that living, crystallization-driven polymerizations has to offer in terms of control and development of exceptional hierarchical micellar architectures. The metallo-BCPs can form semicrystalline micelles by epitaxial crystallization of the core-forming PFS block [75]. This growth process, where the termini of the micelles remain active to the addition of the further PFS BCP unimers can be regarded by analogy as a classical living covalent polymerization. Well-defined micelles with controlled dimensions and a large variety of geometries such as cylinders, platelets, tape-like platelets, pointed-oval-shaped micelles, rods, scarf-shaped micelles have been reported (Fig. 6) [50,74,76–78]. Moreover, these authors have shown that the concept of epitaxial growth of cylindrical micelles can be employed to generate new morphologies from different crystalline substrates in a controlled manner. The growth process can take place from the ends of the crystalline cores of cylindrical micelles or at the edges of platelets, and cylinder–cylinder and platelet-cylinder connections are formed [74].

In most cases, the investigated PFS di-BCP have shown to exhibit seed growth which favors the development of cylindrical or fiber-like micelles. The tendency to form cylinders has been attributed to a counterbalance of the competing effects of the semicrystalline PFS core and intracoronal chain repulsions, thus enforcing the core-corona curvature. Recently, Qian et al. [75] reported a systematic investigation of the factors that affect the self-seeding behavior of the PFS BCP micelles fragments.

Different self-seeding protocols were discussed in details and particular attention was paid to the effect of the annealing conditions. Furthermore, it was demonstrated that at a constant temperature, a subtle tuning of the solvent quality by the addition of a good solvent to the polymer solutions can be used to alter the self-seeding process [75]. In general, a self-nucleation experiment implies that the BCP with an initial crystalline state is heated to a given temperature, denoted as the self-nucleation temperature, that is high enough to melt most of the BCP except a certain number of fragments of the crystallites (denoted as micellar seeds if one refers to BCP solutions) [21,90]. Upon cooling the BCP to lower temperatures, recrystallization takes place employing the seeds which are left unmolten during the heat treatment at the self-nucleation temperature. Hence, crystalline micelles form in solution (see Fig. 7). The authors emphasized that this is not a kinetic effect but rather a thermodynamic one. Moreover, these experiments highlight that the concept of a critical micelle concentration (cmc) or critical micelle temperature (cmt) break down for micelles with a crystalline core.

Usually, the crystal structure and the crystallinity of the core will have a dramatic impact in regulating the micellar architecture. In order to gain knowledge of the crystalline core structure, Gilroy et al. employed SAXS and WAXS techniques to investigate the field-response behavior of cylindrical micelles based on PFS-containing block copolymers [77]. In the presence of an alternating electric field, the micelles revealed a nematic-like phase response with their long axes aligned in the direction of the applied field. From the intensity distribution, the orientation distribution of scattering elements and an order parameter S of 0.77 were determined (see Fig. 6). WAXS data acquired on the same field-aligned sample of cylindrical micelles also revealed that the long axis of the micelles is aligned parallel to the field. The short axis of the cylinders was aligned perpendicular to the field. The authors were able to determine that the PFS-chains packed in a 2D lattice with a pseudo-hexagonal symmetry with characteristic *d*-spacings of 6.29 and 6.43 Å, which was assigned to the interchain packing distances. Additionally, it was shown that the core also possessed an amorphous region near the core-corona/solvent interface. Based on these results, the authors infer that the epitaxial growth process of the PFS segment of the added BCP at the ends of crystalline PFS domains involves an efficient packing (perpendicular to the cylinder long axis) which leads to a controlled growth of the cylinder length.

Moreover, when employed as an additional reservoir to the polymer solution (containing already crystalline micelles), the PFS segment enables the preparation of micelles of controlled dimensions. Yusoff et al. showed that the crystallinity of the added homopolymer to short cylindrical micelles is critical for subsequent end-to-end coupling and network formation [49]. In this case, the deposition and crystallization of a polyferrocenylsilane homopolymer (PFS) at the ends of the cylindrical BCP seed micelles with a PFS core leads to aggregation. As a result, the end-to-end coupling of two or more micelles can give rise to linear, linked or branched structures.

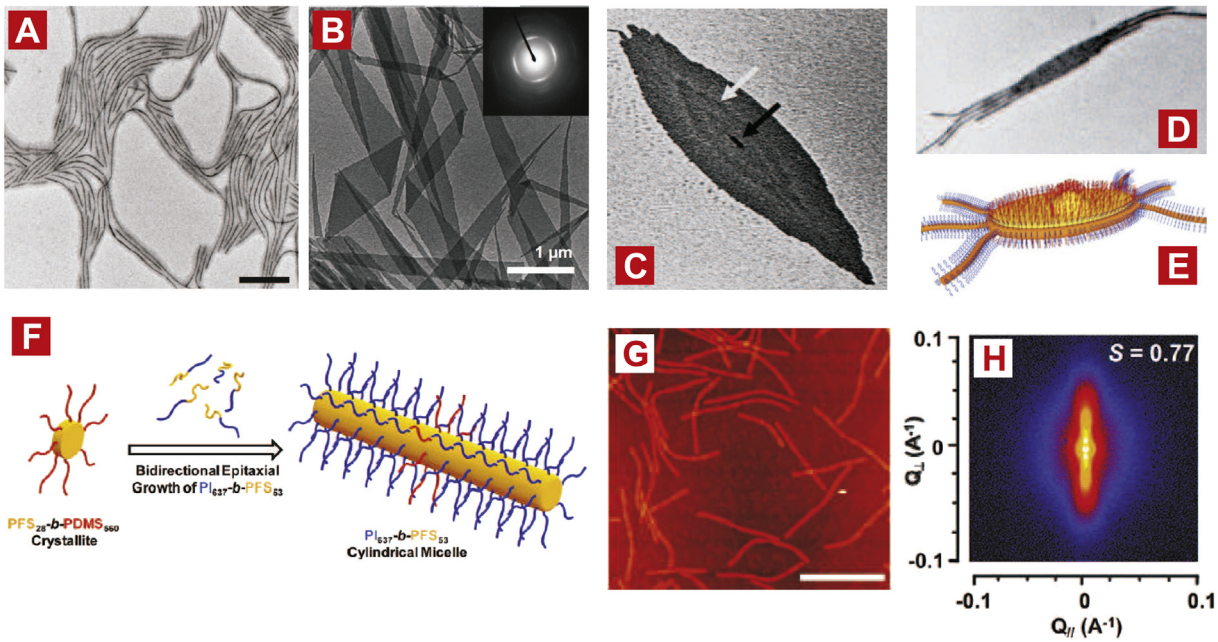

Fig. 6. A) TEM micrograph of semicrystalline cylindrical micelles. Reproduced by permission of The American Chemical Society from Ref. [49]. B) TEM micrograph of a tape-like structure formed by PI-*b*-PFDES BCP in a mixture of decane/xylene. The SAED patter (inset) shows the crystalline nature of the PFDES core of this morphology. Reproduced by permission of The American Chemical Society from Ref. [76]. C) Uniform pointed-oval-like micelles obtained by sequential addition of PFS-*b*-PP unimers (molecularly dissolved BCP in THF, a good solvent for both blocks) to a central PFS-*b*-P2VP short cylindrical seed-micelle (prepared by sonication from longer cylinder micelle dispersion), D) Hierarchical micellar architecture obtained by the epitaxial growth of cylindrical micelles off the pointed-oval-shaped micelles along their long axis, where the ovals were used as precursors, and E) Schematic representation of the complex micellar structure where the crystalline micellar core is represented in orange (central cylinder, ribbon around the pointed oval and cylindrical tassels growing outside the pointed oval,PFS-*b*-P2VP) and yellow (body of the pointed oval of PFS-*b*-PP). Copyright 2010 WILEY-VCH Verlag GmbH & Co. KGaA [50]. F) Crystalline micelles formation through bidirectional epitaxial growth from stub-like crystallites. Reproduced by permission of The American Chemical Society from Ref. [77]. G) AFM height image of PI_{637}-*b*-PFS_{53} (the subscripts refer to the number average degree of polymerization) cylindrical micelles and H) SAXS pattern of PI_{637}-*b*-PFS_{53} cylindrical micelles indicating their alignment in the presence of an electric field of 4.0 $V\mu m^{-1}$. The orientational order parameter, S, of the rods was determined to be 0.77. Reproduced with permission of The American Chemical Society from Ref. [77]. (For interpretation of the references to color in this figure legend, the reader is referred to the web version of this article.)

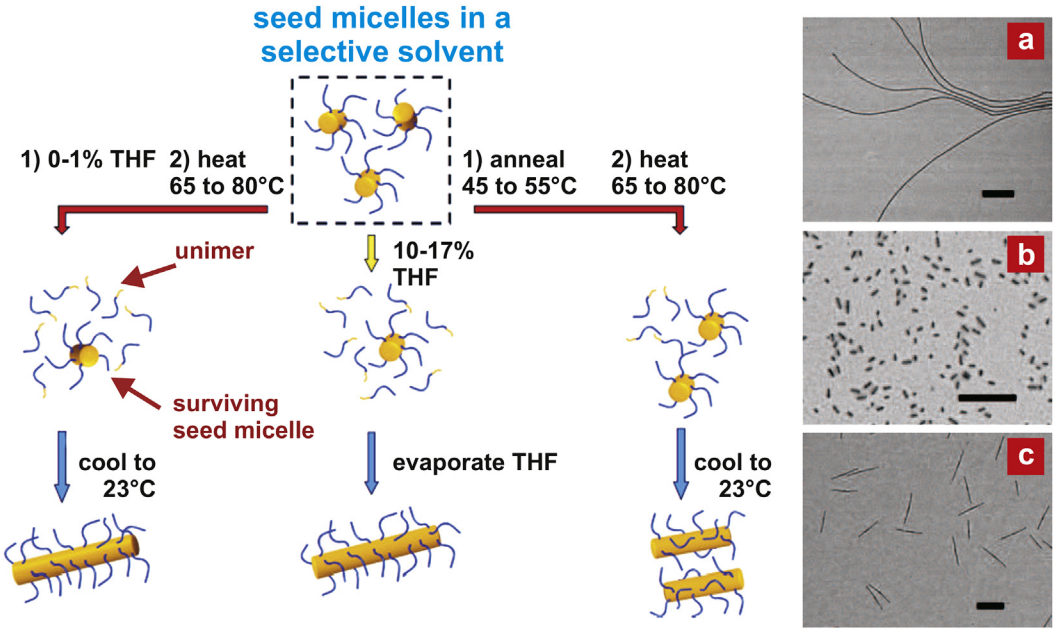

Fig. 7. Self-seeding protocols proposed by Qian et al. [75] to prepare crystalline micelles with well-distributed lengths in a selective solvent. Selected examples of micelles obtained by employed self-seeding protocols from polyisoprene-*b*-poly(ferrocenyldimethylsilane) (PI-PFS) BCP: a) by slow cooling of the hot polymer solution from 100 °C to room temperature (the polymer was dissolved in decane); b) micelle fragments obtained by sonicating the long micelles in a), and c) by cooling to room temperature the micelles fragments containing 1 vol% THF that were previously kept at 70 °C for 30 min. Reprinted with permission from Ref. [75]; Copyright 2013 American Chemical Society.

Micellar growth driven by epitaxial crystallization of the core-forming PCL block of cylindrical PCL-*b*-PEO micelles has been observed in different mixed solvents [79]. Xu et al. investigated the growth mechanism from different seed micelles such as amorphous spherical micelles, mixtures of amorphous spheres and short semicrystalline cylinders or uniform short cylinders. A "self-seeding-like" method was used to prepare the semicrystalline micellar seeds for further micellar growth. In this case, the micellar solutions were held at a temperature near the melting temperature of the PCL block for a given time. In addition to the micellar semicrystalline seeds, amorphous micelles and unimers were found to coexist in the solution. Upon cooling to the crystallization temperature, the nucleation and growth process started from the crystalline remains or seeds which resisted to the previous melting procedure, generating larger cylindrical micelles. To avoid any stability problems due to a decreased solubility of the PEO corona at high temperatures, different organic solvents including THF, dioxane, DMF and DMSO were added into the aqueous micellar solutions. Thus, manipulation of the growth kinetics was possible. It should be pointed out that two different growth pathways were observed for this BCP: epitaxial crystallization growth of unimers or amorphous spherical micelles on the active ends of the semicrystalline cylindrical seeds, and an end-to-end growth by coupling of different semicrystalline cylindrical micelles. The latter one is slower than the growth of amorphous micelles on the crystalline seeds. This fact is related to the high mobility of the unimers in the solution where they can easily get attached to the ends of the crystalline seeds, whereas for the second growth mode, the coupling is possible only when the ends of two short cylinders meet. Through this manipulation the cylindrical micelles can further grow into fiber-like micelles while preserving a constant diameter.

Lately, non-centrosymmetric structures became accessible from a living CDSA approach [92]. These BCP structures are especially attractive for the bottom-up design of hierarchical assemblies. Multi-armed micelles were obtained by the crystallization-driven growth of poly(ferrocenyl-dimethylsilane)-*b*-polyisoprene (PFS-*b*-PI) cylindrical micelles from seed nanocrystals of the PFS homopolymer [66]. These micelles possessed a hierarchical multipod structure with monodisperse and tunable arm lengths that remain active for further chemistry. Moreover, branched segmented hybrid structures can be obtained by selectively crosslinking the PI coronar chains of the arm segments. The authors claimed that this principle should be applicable to other crystalline coil-BCPs, where one can create hierarchical morphologies by driving the crystallization process from the corresponding homopolymer nanocrystals as seeds. By doing so, the authors showed that epitaxial growth from active termini of seeds is no longer restricted to one-dimensional growth.

The CDSA of poly(lactide) (PLA)-containing block copolymers through a thermally controlled crystallization (above the glass transition temperature of the core) enabled the preparation of well-defined cylindrical micelles of controlled dimensions via a living epitaxial growth [93]. Moreover, the length of the resulting cylinders can be varied by altering the hydrophilic character of the corona-forming block [94]. The more hydrophilic corona has led to the shortest cylinders. The addition speed of the selective solvent plays also a crucial role in order to attain cylindrical micelles with a narrow distribution in length in the final state.

3. Hybrid materials: when colloidal particles meet BCP micelles with a crystalline corona

In the following we will show that crystallization-driven self-assembly can be regarded as an innovative associative strategy also for the development of hybrid inorganic-organic materials. In all the examples mentioned above, the CDSA method has been employed to generate micellar BCP morphologies containing crystalline-core forming blocks. Recently, Mihut and co-workers showed that this assembly strategy can be extended to BCP which can crystallize in the micellar corona instead of the core and additionally drive self-assembly of colloidal particles [91]. A semicrystalline PB-*b*-PEO BCP in ethanol at 60 °C, that is, above T_m of the PEO block, forms amorphous spherical micelles consisting of a liquid PEO-corona and a PB-core. Ethanol is a poor solvent for the PB block and a selective solvent for the PEO block. Below T_m, the PEO crystallizes in the micellar corona at lower temperatures and leads to the formation of lamellar structures. Therefore, when silica nanoparticles (NPs) were added to the warm BCP solutions, the crystallization process dictated the spatial distribution and the self-assembly of the colloidal particles into the BCP lamellar domains. Under these conditions, the crystallization process of the PEO block in the micellar corona proved to be an effective strategy to generate different hybrid assemblies. Such association is tunable and reversible, following the crystallization temperature T_m.

Hybrid supramolecular assemblies such as dendrites and lamellae of colloidal silica NPs covered by the PB_{48}-*b*-$PEO_{58}^{10.6}$ BCP (the subscripts denote the mass fraction in percent and the superscript gives the overall number average molecular weight of the block copolymer in kg/mol) were obtained in dilute solutions via different crystallization pathways where the quench depth and rate was varied (Fig. 8). The red spots (in web version) in Fig. 8 represent the regions where fluorescent silica NPs were detected by confocal laser scanning microscopy (CLSM), indicating the arrangement of the colloidal particles in the hybrid suspensions. Once the PEO block copolymer is no longer confined within the spherical micellar domains in which it nucleate, *i.e.*, breakout from the melt morphology occurs upon crystallization which leads to the formation of larger morphological structures. A similar behavior where crystallization and aggregation of spherical micelles take place side-by-side has been observed for PB_{52}-*b*-$PEO_{48}^{5.6}$ BCP in *n*-heptane [56,58]. SAXS measurements on the silica/PB_{52}-*b*-$PEO_{48}^{5.6}$ BCP mixtures indicated the presence of lamellar structures with an interlamellar distance (*d*-spacing between two lamellae) of 26.2 nm, whereas the TEM micrographs revealed 28 nm. Moreover, the lamellar structure remained almost unperturbed upon the PEO crystallization at distinct T_c. These features are a direct consequence of the combination of two coupled processes, that is, the crystallization-driven self-assembly (CDSA) of the BCP micelles and the guided self-assembly of the colloidal silica NPs. The NPs are incorporated within the crystalline BCP lamellar structure and their localization is not arbitrary. There is a certain affinity between the NPs and the BCP micelles related to the hydrogen bond formation between the ether oxygens of the PEO and the silanol groups at the silica surface. Hence, the onset of crystallization at different T_c in the micellar corona is the driving force for the colloidal self-assembly. Similar self-assembly behavior was observed in ethanol for another PB-*b*-PEO BCP when varying the molecular weight and block ratios. Dendritic hybrid structures were obtained by fast crystallization of the mixture of colloidal silica NPs/PB_{62}-*b*-$PEO_{38}^{10.4}$ BCP at 4 °C (Fig. 9). Interestingly, a careful examination of the 3D CLSM projection evidences that these structures are composed of domains which extend in solution over a few micrometers as shown in Fig. 9B.

It can be emphasized that under these conditions, the self-assembly of the colloidal particles is guided by the crystallization process into a preferential direction at the crystal growth front. As a result, the silica NPs assembled in a regular manner of string-like aggregates into the hybrid morphologies. By doing so, novel nano- and microstructured hybrid block copolymer-nanoparticle

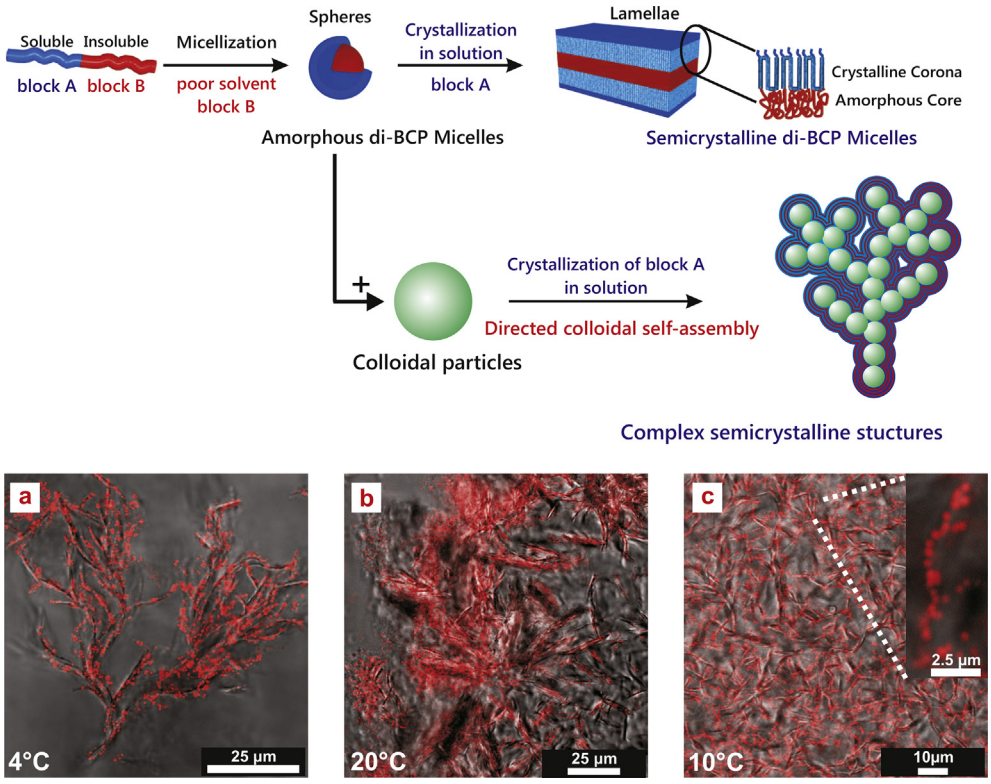

Fig. 8. Schematic drawing illustrating the hybrid assemblies fabrication of crystalline BCP micelles and silica particles. Below 60 °C, the PEO-corona forming block undergoes crystallization. The onset of crystallization at different T_c in the micellar corona is the driving force for the colloidal self-assembly. a)–c): Hybrid assemblies formed by PB-*b*-PEO BCP/silica colloidal particles at different crystallization temperatures and cooling rates. Adapted from Ref. [91]; Copyright 2013, Elsevier.

materials with large internal interfaces and connected hybrid compartments are becoming accessible, where the integration of the NPs is no longer restricted to the microphase separation of the block copolymer.

CDSA of polythiophene-containing block copolymers has proven already exceptionally useful for preparing functional or hybrid materials with interesting nanostructures and optoelectronic properties for potential applications such as field-effect transistors and solar cells [95]. Among a large variety of morphologies formed by the π-conjugated polymers, fiber-like micelles containing a conductive core are of particular interest as conductive nanowires for different applications [96]. Generally, the device performance and efficiency is a subtle balance of polymer crystallinity and morphology. Qian et al. have shown that uniform fiber-like micelles containing a relatively defect-free crystalline core can be generated by using a self-seeding approach [97]. The crystallization of π-conjugated polymers in solution also enabled the fabrication of organic-inorganic hybrid nanowires containing segregated heterojunctions between the crystalline polymer and the inorganic particles [98–100]. Recently, Kim et al. showed that CDSA leads to hybrid nanowire formation with controlled location of the inorganic quantum dot arrays within the coaxial hybrid

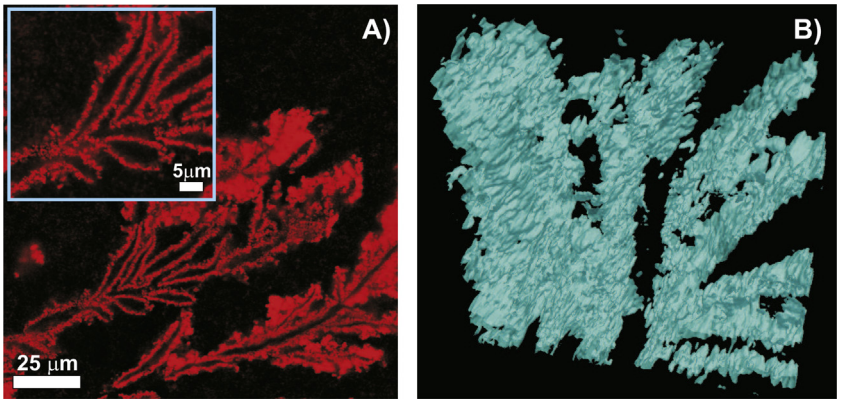

Fig. 9. Hybrid assemblies of silica NPs/PB_{62}-*b*-$PEO_{38}^{10.4}$ BCP formed in ethanol solution by fast crystallization to 4 °C: A) CLSM and B) 3D projection of the same morphology as in A) which was reconstructed from confocal z-stack images ($24.6 \times 24.6 \times 7.06\ \mu m^3$. The subscripts denote the mass fraction in percent and the superscript gives the overall number average molecular weight of the block copolymer in kg/mol. The molecular weights of the PB and PEO blocks are 6.5 kg/mol and 3.9 kg/mol, respectively. The red (A) and blue (B) represent the regions where fluorescent silica NPs were detected. (For interpretation of the references to color in this figure legend, the reader is referred to the web version of this article.)

nanowires [101]. Therefore, the CDSA approach offers a large potential within nanotechnology applications through the selection of the incorporated nanoparticles with magnetic, catalytic or optical properties, which can respond effectively to external stimuli, or by the choice of the type of crystalline block copolymer (such as semiconductive or metallosupramolecular blocks) [95].

4. Conclusions and future perspectives

The self-assembly and the development of semicrystalline block copolymer micelles can be in general achieved either by a thermally controlled crystallization, where one can vary the crystallization conditions by imposing a certain crystallization temperature, or by an epitaxial crystallization where a self-seeding like method is employed to prepare micellar crystalline seeds for further micellar growth. Taking advantage of these methods and the large diversity of existing block copolymers that are able to crystallize, one can begin to manipulate the micellar diblock copolymer morphology and to tune the selectivity of desired materials. Therefore, these approaches can be applied as efficient and versatile fabrication methods to achieve morphological control not only in terms of size and shape but also in hierarchical complexity. Overall, we can conclude that the micellar morphology is strongly influenced by different relevant parameters such as the crystallization temperature and kinetics, the effect of solvent solubility, or the influence of the BCP molecular composition. These findings demonstrate the great potential that this field has to offer in the future, as the morphology is no longer restricted to the intrinsic molecular parameters of the BCP and alternative routes of controlling the micellar structures can be achieved by tuning the BCP chains interactions either in the core or in the corona. However, experimental and theoretical phase diagrams of either dilute or concentrated semicrystalline micellar systems are still unexplored.

If to date the main targeted effort was focused on the development of new effective strategies to generate materials in desired geometries and to tune the final structure by understanding their behavior in solution, the next step would be to focus on novel exploratory studies that emphasize their response to external parameters other than the temperature. The design of a wide range of structures often reversible and tunable as a function of temperature, makes them promising candidates in applications that will require for example enhanced mechanical reliability. Moreover, due to their biocompatibility and biodegrability, some of these semicrystalline BCP micelles could be suitable candidates in biomedical fields as drug carriers. Additionally, the preparation of hybrid materials containing semicrystalline micelles/inorganic colloids enables the development of a new generation of materials and devices if the crystallization-driven self-assembly process is applied to semiconductive BCPs or to nanoparticles which possess magnetic or optical properties.

Acknowledgments

We gratefully acknowledge financial support from the Faculty of Science of Lund University, and the Swedish Research Council VR through the Linnaeus Center of Excellence on Organizing Molecular Matter.

References

[1] Smart T, Lomas H, Massignani M, Flores-Merino MV, Perez LR, Battaglia G. Nanotoday 2008a;3:38–46.
[2] Kim JK, Yang SY, Lee Y, Kim Y. Prog Polym Sci 2010;35:1325–49.
[3] Alexandridis P, Lindman B. Amphiphilic block copolymers: self-assembly and applications. 1st ed. Amsterdam: Elsevier; 2000.
[4] Hamley IW. Block copolymers in solution: fundamentals and applications. 1st ed. Chichester, UK: John Wiley & Sons. Ltd; 2005.
[5] Smart T, Lomas H, Massignani M, Flores-Merino MV, Perez LR, Battaglia G. Nanotoday 2008b;3:38–46.
[6] Jain S, Bates FS. Science 2003;300:460–4.
[7] Wang X, Goswami M, Kumar R, Sumpter BG, Mays J. Soft Matter 2012;8:3036–52.
[8] Simone PM, Lodge TP. Macromolecules 2008;41:1753–9.
[9] Israelachvili J. Intermolecular & surface forces. 2nd ed. London: Academic Press; 1991.
[10] Riess G. Prog Polym Sci 2003;28:1107–70.
[11] Hellweg T. Adv Polym Sci 2011;242:1–27.
[12] Blanazs A, Armes SP, Ryan AJ. Macromol Rapid Commun 2009;30:267–77.
[13] Milchev A, Bhattacharya A, Binder K. Macromolecules 2001;34:1881–93.
[14] Hayward RC, Pochan DJ. Macromolecules 2010;43:3577–84.
[15] Zhulina EB, Borisov OV. Macromolecules 2012;45:4429–40.
[16] Vilgis T, Halperin A. Macromolecules 1991;24:2090–5.
[17] Mihut AM, Crassous JJ, Schmalz H, Drechsler M, Ballauff M. Soft Matter 2012;8:3163–73.
[18] Müller AJ, Arnal ML, Trujillo M, Lorenzo AT. Eur Polym J 2011;47:614–29.
[19] Castillo R, Müller A. Prog Polym Sci 2009;34:516–60.
[20] Müller AJ, Arnal ML, Balsamo V. Lect Notes Phys 2007;714:229–59.
[21] Müller AJ, Balsamo V, Arnal ML. Adv Polym Sci 2005;190:1–63.
[22] Darko C, Botiz I, Reiter G, Breiby DW, Andreasen JW, Roth SV, et al. Phys Rev E 2009;79. 041802(1)–041802(5).
[23] Reiter G, Vidal L. Eur Phys J E 2003;12:497–505.
[24] Reiter G, Vidal L. Polymer 2005;46:4868–75.
[25] Loo YL, Register RA, Ryan AJ. Macromolecules 2002;35:2365–74.
[26] Zhao J, Zhang J, Duan X, Peng Z, Wang S. Polymer 2011;52:2085–93.
[27] Vasilev C, Reiter G, Pispas S, Hadjichristidis N. Polymer 2006;47:330–40.
[28] Reiter G. Chem Soc Rev 2014;43:2055–65.
[29] Michell RM, Blaszczyk-Lezak I, Mijangos C, Müller AJ. Polymer 2013;54:4059–77.
[30] Müller AJ, Arnal ML, Lorenzo AT. Handbook of polymer crystallization. Hoboken, NJ, USA: John Wiley & Sons, Inc.; 2013. http://dx.doi.org/10.1002/9781118541838.ch12.
[31] Michell RM, Blaszczyk-Lezak I, Mijangos C, Müller AJ. J Polym Sci Part B: Polym Phys 2014;52:1179–94.
[32] Du ZX, Xu JT, Fan ZQ. Macromol Rapid Commun 2008;29:467–71.
[33] Du ZX, Xu JT, Fan ZQ. Macromolecules 2007a;40:7633–7.
[34] Yin L, Lodge TP, Hillmyer MA. Macromolecules 2012;45:9460–7.
[35] He WN, Xu JT, Du BY, Fan ZQ, Sun FL. Macromol Chem Phys 2012a;213:952–64.
[36] Schmelz J, Schmalz H. Polymer 2012;53:4333–7.
[37] Schmelz J, Schacher FH, Schmalz H. Soft Matter 2013;9:2101–7.
[38] Schmalz H, Schmelz J, Drechsler M, Yuan J, Walther A, Schweimer K, et al. Macromolecules 2008;41:3235–42.
[39] Schmelz J, Karg M, Hellweg T, Schmalz H. ACS Nano 2011;5:9523–34.
[40] He WN, Xu JT. Prog Polym Sci 2012;37:1350–400.
[41] Richter D, Schneiders D, Monkenbusch M, Willner L, Fetters LJ, Huang JS, et al. Macromolecules 1997;30:1053–68.
[42] Massey JA, Temple K, Cao L, Rharbi Y, Raez J, Winnik MA, et al. J Am Chem Soc 2000a;122:11577–84.
[43] Shen L, Wang H, Guerin G, Wu C, Manners I, Winnik M. Macromolecules 2008a;41:4380–9.
[44] Raez J, Tomba JP, Manners I, Winnik MA. J Am Chem Soc 2003;125:9546–7.
[45] Raez J, Manners I, Winnik MA. Langmuir 2002a;18:7229–39.
[46] Wang X, Wang H, Frankowski DJ, Lam PG, Welch PM, Winnik MA, et al. Adv Mater 2007a;19:2279–85.
[47] Gädt T, Ieong NS, Cambridge G, Winnik MA, Manners I. Nat Mater 2009a;8:144–50.
[48] Lazzari M, Scalarone D, Vazquez-Vazquez C, Lopez-Quintela MA. Macromol Rapid Commun 2008;29:352–7.
[49] Yusoff SFM, Gilroy JB, Cambridge G, Winnik MA, Manners I. J Am Chem Soc 2011;133:11220–30.
[50] Soto AP, Gilroy JB, Winnik MA, Manners I. Angew Chem Int Ed 2010;49:8220–3.
[51] He F, Gädt T, Manners I, Winnik MA. J Am Chem Soc 2011;133:9095–103.
[52] Yin L, Hillmyer MA. Macromolecules 2011;44:3021–8.
[53] Chen SC, Wu G, Shi J, Wang YZ. Chem Commun 2011;47:4198–200.
[54] He WN, Xu JT, Du BY, Fan ZQ, Sun FL. Macromol Chem Phys 2012b;213:952–64.
[55] Gilroy JB, Gädt T, Whittell GR, Chabanne L, Mitchels JM, Richardson RM, et al. Nat Chem 2010;2:566–70.
[56] Mihut AM, Chiche A, Drechsler M, Schmalz H, Cola ED, Krausch G, et al. Soft Matter 2009;5:208–13.
[57] Mihut AM, Drechsler M, Möller M, Ballauff M. Macromol Rapid Commun 2010a;31:449–53.
[58] Mihut AM, Crassous JJ, Schmalz H, Ballauff M. Colloid Polym Sci 2010b;288:573–8.
[59] Li Z, Liu R, Mai B, Wang W, Wu Q, Liang G, et al. Polymer 2013a;54:1663–70.
[60] Liu R, Li ZY, Mai BY, Wu Q, Liang GD, Gao HY, et al. J Polym Res 2013a;20.64(1)–(11).
[61] Liu R, Li ZY, Wang WJ, Yuan D, Meng CF, Wu Q, et al. J Appl Polym Sci 2013b;129:2216–23.

[62] Schacher FH, Freiera U, Steiniger F. Soft Matter 2012;8:2968–78.
[63] Wang H, Liu CL, Wu G, Chen SC, Songa F, Wang YZ. Soft Matter 2013;9:8712–22.
[64] Pitto-Barry A, Kirby N, Dove AP, OReilly RK. Polym Chem 2014a;5:1427–36.
[65] Hsiao MS, Yusoff SFM, Winnik MA, Manners I. Macromolecules 2014;47:2361–72.
[66] Qiu H, Cambridge G, Winnik MA, Manners I. J Am Chem Soc 2013;135:12180–3.
[67] Rizis G, van de Ven TGM, Eisenberg A. Angew Chem Int Ed 2014;53:1–5.
[68] Su M, Huang H, Ma X, Wang Q, Su Z. Macromol Rapid Commun 2013;34:1067–71.
[69] He WN, Xu JT, Du BY, Fan ZQ, Wang X. Macromol Chem Phys 2010;211:1909–16.
[70] Shen L, Wang H, Guerin G, Wu C, Manners I, Winnik MA. Macromolecules 2008b;41:4380–9.
[71] Massey J, Temple K, Cao L, Rharbi Y, Raez J, Winnik MA, et al. J Am Chem Soc 2000b;122:11577–84.
[72] Raez J, Manners I, Winnik MA. J Am Chem Soc 2002b;124:10381–95.
[73] Li Z, Liu R, Mai B, Feng S, Wu Q, Liang G, et al. Polym Chem 2013b;4:954–60.
[74] Gädt T, Ieong NS, Cambridge G, Winnik MA, Manners I. Nat Mater 2009b;8:144–50.
[75] Qian J, Lu Y, Chia A, Zhang M, Rupar PA, Gunari N, et al. ACS Nano 2013;7:3754–66.
[76] Gädt T, Schacher FH, McGrath N, Winnik MA, Manners I. Macromolecules 2011;44:3777–86.
[77] Gilroy JB, Rupar PA, Whittell GR, Chabanne L, Terrill NJ, Winnik MA, et al. J Am Chem Soc 2011;133:17056–62.
[78] Wang X, Wang GGH, Wang Y, Manners I, Winnik MA. Science 2007b;317:644–7.
[79] He WN, Zhou B, Xu JT, Du BY, Fan ZQ. Macromolecules 2012c;45:9768–78.
[80] Xu JT, Jin W, Liang GD, Fan ZQ. Polymer 2005;46:1709–16.
[81] Du ZX, Xu JT, Fan ZQ. Macromolecules 2007b;40:7633–7.
[82] Petzetakis N, Walker D, Dove AP, OReilly RK. Soft Matter 2012;8:7408–14.
[83] Rider DA, Winnik MA, Manners I. Chem Commun 2007;43:4483–5.
[84] Rider DA, Chen JIL, Eloi JC, Arsenault AC, Russell TP, Ozin GA, et al. Macromolecules 2008;41:2250–9.
[85] Hinderling C, Stöckli YKT, Knapp HF, de los Arcos T, Oelhafen P, Korczagin I, et al. Adv Mater 2004;16:876–9.
[86] Lastella S, Jung YJ, Yang H, Vajtai R, Ajayan PM, Ryu CY, et al. J Mater Chem 2004;14:1791–4.
[87] Korczagin I, Lammertink RGH, Hempenius MA, Golze S, Vancso GJ. Adv Polym Sci 2006;200:91–117.
[88] Eitouni HB, Balsara NP. J Am Chem Soc 2006;128:16248–52.
[89] Li JK, Zou S, Rider DA, Manners I, Walker GC. Adv Mater 2008;20:1989–93.
[90] Xu J, Ma Y, Hu W, Rehahn M, Reiter G. Nat Mat 2009a;8:348–53.
[91] Mihut AM, Crassous JJ, Dechézelles JF, Lages S, Menzel A, Dietsch H, et al. Polymer 2013;54:3874–81.
[92] Rupar PA, Chabanne L, Winnik MA, Manners I. Science 2012;337:559–62.
[93] Petzetakis N, Dove AP, OReilly RK. Chem Sci 2011;2:955–60.
[94] Pitto-Barry A, Kirby N, Dove AP, OReilly RK. Polym Chem 2014b;5:1427–36.
[95] Emrick T, Pentzer E. NPG Asia Mater 2013;5:e43. http://dx.doi.org/10.1038/am.2012.73.
[96] Gwyther J, Gilroy JB, Rupar PA, Lunn DJ, Kynaston E, Patra SK, et al. Chem Eur J 2013;19:9186–97.
[97] Qian J, Li X, Lunn DJ, Gwyther J, Hudson ZM, Kynaston E, et al. J Am Chem Soc 2014;136:4121–4.
[98] Xu J, Hu J, Liu X, Qiu X, Wei Z. Macromol Rapid Commun 2009b;30:1419–23.
[99] Bokel FA, Sudeep PK, Pentzer E, Emrick T, Hayward RC. Macromolecules 2011;44:1768–70.
[100] Pentzer EB, Bokel FA, Hayward RC, Emrick T. Adv Mater 2012;24:2254–8.
[101] Kim YJ, Cho CH, Paek K, Jo M, kyoung Park M, Lee NE, et al. J Am Chem Soc 2014;136:2767–74.

Jérôme J. Crassous has a researcher position since 2013 at the Division of Physical Chemistry at Lund University, Sweden. He got his M.Sc. in Material Science at INSA-Lyon (University of Lyon, France) in 2003 and his PhD at the University of Bayreuth, Germany, under the supervision of Prof. Matthias Ballauff in 2009 at the Department of Physical Chemistry I. He was a postdoctoral fellow in the group of Prof. Peter Schurtenberger at the Adolphe Merkle Insitute (University of Fribourg, Switzerland) in 2009 and then moved in 2011 to Lund University, Sweden. His research interests are focused on complex directed self-assembly processes mostly based on responsive colloids and on the physical properties of dense colloidal dispersions.

Peter Schurtenberger is a Professor in Physical Chemistry at the Division of Physical Chemistry at Lund University. He received his PhD from the Swiss Federal Institute of Technology (ETH) in Zurich in 1984. After working as a postdoc at Lund University, Sweden, MIT and Harvard University Medical School, he spent 12 years as a senior researcher at the Department of Materials of ETHZ. In 1999 he was appointed as the chair in experimental soft matter physics at the University of Fribourg. In 2006 he founded the Fribourg Center for Nanomaterials, and became the first director of the newly founded Adolphe Merkle Institute for Pure and Applied Nanoscience in 2008. He moved to Lund University at the end of 2010. He has been elected as a member of the Royal Swedish Academy of Sciences, is a Fellow of the Royal Society of Chemistry, and honorary member of the European Colloid and Interface Society. He is co-founder and board member of the company LS Instruments.

Matthias Ballauff studied chemistry at the University of Mainz and got is PhD there in the Institute of Physical Chemistry in 1981. He was a postdoc in the group of P.J. Flory in Stanford from 1981 to 1983 and subsequently research associate at the Max-Planck-Institute for Polymer Research in Mainz. From 1990 to 2003 he was a professor of polymer science at the University of Karlsruhe. From 2003 to 2009 he hold the chair of Physical Chemistry I at the University of Bayreuth. From 2009 on he is a professor of Experimental Physics at the Humboldt University Berlin and Head of the Institute of Soft Matter and Functional Materials at the Helmholtz-Zentrum Berlin. His interests comprise scattering methods and polymer colloids for applications in materials science and catalysis.

Adriana M. Mihut obtained her PhD from the University of Bayreuth, Germany (2010) under the direction of Prof. Matthias Ballauff. Her thesis focused on the crystallization-driven self-assembly of poly (ethylene oxide) containing block copolymers in selective solvents. After working as a postdoc at Adolphe Merkle Institute, University of Fribourg, Switzerland (2010–2011), she joined since 2012 the group of Prof. P. Schurtenberger at Lund University, Sweden. Her research interests covers block copolymer self-assembly, interactions of colloidal particles with model biomembranes, the synthesis of responsive colloids and their directed self-assembly.